CHEMISTRY
A EUROPEAN JOURNAL

DOI: 10.1002/chem.200600088

Controlled Assembly of a Heterogeneous Single-Site Ethylene Trimerization Catalyst as Probed by X-ray Absorption Spectroscopy

Cristina N. Nenu,[a] Joost N. J. van Lingen,[a, b] Frank M. F. de Groot,[a] Diek C. Koningsberger,[a] and Bert M. Weckhuysen*[a]

Abstract: X-ray absorption spectroscopy at the Cr K- and $L_{2,3}$-edges was used to study the assembling process of a heterogeneous Cr-based single-site catalyst. The starting point was a Phillips-type system with monochromate species anchored on a silica surface, which was first reduced to a variety of different surface Cr^{II} species. The reduced sample was modified with a 1,3,5-tribenzylhexahydro 1,3,5-triazine (TAC) ligand in the presence of CH_2Cl_2 as solvent to yield a heterogeneous single-site Cr-based catalyst active in the trimerization of ethylene. The molecular structure of the resultant catalytic material consists of distorted octahedral Cr^{III} species. The extended X-ray absorption fine-structure (EXAFS) spectroscopy fitting procedure in *R* space up to 2.5 Å showed that the synthesis leads to coordination with a TAC ligand. The fit also shows that it was possible to complete the six-fold environment around Cr^{III} with two oxygen atoms and one chloride ligand. This chloride ligand is formed in a redox process from the solvent and is responsible for the oxidation of surface Cr^{II} to Cr^{III}. The obtained geometry and the local environment of the surface complex are discussed in light of its homogeneous counterpart and confirm the single-site characteristics of the prepared catalytic material.

Keywords: chromium · heterogeneous catalysis · Phillips catalyst · polymerization · X-ray absorption spectroscopy

Introduction

The aim of catalyst scientists is to control the synthesis of the active site of a heterogeneous catalyst, as well as the environment of the active site and the access to it.[1,2] Unfortunately, single-site heterogeneous catalysts have been obtained in only a few cases,[3] and usually, one ends up with a broad distribution of active sites.[4] An example of this is the Phillips polymerization catalyst, which is composed of a chromium oxide supported on a silica carrier.[1–7] This catalyst, responsible for about 40% of the worldwide production of polyethylene,[1–7] is characterized by large polydispersity indexes (PDI) of 6–15.[8–13] Such high values (single-site catalysts have typical PDI indexes of around 1–4) indicate that each active site has its own specific catalytic behavior, leading to the production of different polyethylene chains and, therefore, to a broad molecular-weight distribution. Hence, it is not surprising that in spite of many efforts in catalyst characterization over the last four decades, there is still a lot of controversy regarding the active site and the related reaction mechanism of Phillips-type polymerization catalysts.[5–10]

Cr^{II} is generally considered as the active site in polymerization processes, although several different Cr^{II} structures were identified by using the in situ infrared CO-adsorption technique and labeled as Cr^{II}_A, Cr^{II}_B, Cr^{II}_C, and Cr^{II}_D. Besides, chromium sites in the oxidation state of three, four, and five may coexist. Evidently, such a complex system is difficult to investigate and methods to reduce or, if possible, to remove its complexity should be developed. McDaniel[12,13] was the first to report on a method with CO at elevated temperature in which Cr^{II}_A sites are almost integrally converted into Cr^{II}_B sites. The polydispersion of the system is modestly reduced. Another approach to increase the homogeneity of the surface was recently investigated by Zec-

[a] C. N. Nenu, J. N. J. van Lingen, Dr. F. M. F. de Groot, Prof. Dr. D. C. Koningsberger, Prof. Dr. B. M. Weckhuysen
Inorganic Chemistry and Catalysis, Department of Chemistry
Utrecht University, PO Box 80083
3508 TB Utrecht (The Netherlands)
Fax: (+31) 302-531-027
E-mail: b.m.weckhuysen@chem.uu.nl

[b] J. N. J. van Lingen
Theoretical Chemistry Group (Affiliated to Organic Chemistry and Catalysis), Department of Chemistry
Utrecht University, PO Box 80083
3508 TB Utrecht (The Netherlands)

Supporting information for this article is available on the WWW under http://www.chemeurj.org/ or from the author.

china and co-workers.[14] They succeeded in partially converting Cr^{II}_A species into Cr^{II}_B species simply by using thermal treatments after the reduction step. Both approaches are based on the tendency of naked Cr^{II}_A sites to seek potential vicinal ligands and to consequently sink into the superficial layer of the silica lattice to reduce their high degree of unsaturation. In other words, Cr finds a better position on the surface and becomes better coordinated, and, thus, more stable. In fact, these methods were focused on only Cr^{II}_A and Cr^{II}_B sites, and are, therefore, incomplete as long as Cr^{II}_C, Cr^{II}_D sites and different structures of Cr^{II}_B sites still exist on the surface. Another interesting approach by the groups of Niemantsverdriet[15–20] and Grange[21,22] has targeted this complexity issue by spin coating a Cr precursor on SiO_2/Si(100) wafers, aiming to reduce the number of polymerization centers as well as to form isolated Cr^{II} polymerization centers. The latter allows the formation of polyethylene islands to be monitored by using scanning force microscopy.

In a recent communication and related patent application,[23,24] we reported briefly on a novel TAC-modified Cr/SiO_2 catalyst that is very active and selective in the trimerization of ethylene, with activities well above those of its homogeneous counterpart. Specific tests also showed that the catalyst is truly heterogeneous and, therefore, its remarkable catalytic activity is due to newly Cr-assembled surface species. However, more intriguing is that the catalyst possesses a polydispersity index of 1.87, indicative of the single-site catalytic behavior. Despite its outstanding catalytic properties, the molecular structure of the active site is unknown. Moreover, this novel catalyst system is ideally suited for a detailed characterization study because data analysis is relatively straightforward compared with those systems involving a broad spectrum of active Cr^{II} sites.

Here, we present a full account and show that a broad distribution of active Cr^{II} sites in Phillips-type Cr/SiO_2 catalysts can be significantly reduced by anchoring a 1,3,5-tribenzylhexahydro 1,3,5-triazine (TAC) ligand and chloride ligands onto the surface Cr species. The reduction in the polydispersity and the assembling process of the new active sites are depicted in Scheme 1. X-ray absorption spectroscopy and DFT calculations were used to unravel the assembling process of the ethylene-trimerization site and to elucidate the geometry and the local environment of the active site of this catalytic system. The results are discussed in relation to the complex surface chemistry of reduced Cr species, usually observed for Phillips-type catalysts.

Experimental Section

Catalyst preparation: Catalyst preparation began with the anchoring of 1 wt% CrO_3 (p.a., UCB) onto silica through esterification with its silanol groups, after calcination at 720 °C. The silica support had a surface area of 500 $m^2 g^{-1}$, a pore volume of 1.5 $mL g^{-1}$, a purity of 99.6% and an isoelectric point of 3.2. After calcination, the yellow-orange material (sample A, Scheme 1) was reduced in either CO or H_2 and the solid turned blue, due to Cr^{II} formation (sample B, Scheme 1). Reduction was followed by coordination of the ligand to the reduced Cr center after impregnation of the pore volume with a solution of the 1,3,5-tribenzylhexahydro 1,3,5-triazine ligand (TAC) in a chlorinated solvent, such as dichloromethane (Aldrich, 99.99% purity, oxygen- and water-free). A light-purple solid was obtained after solvent removal (sample C, Scheme 1).

All treatments were carried out in a specially designed spectroscopic cell that allowed electronic as well as Raman spectra of the solid to be measured. Impregnation of the pore volume was performed under inert atmosphere because of the moisture sensitivity of Cr^{II}. In this respect, it was noted that the as-prepared solid was also sensitive to water. Treatment of the catalyst with a water-saturated gas stream caused a color change to olive-green due to reoxidation of Cr^{II} to Cr^{VI} and the partial formation of Cr_2O_3. Consequently, all further manipulations were carried out under nitrogen atmosphere within a glove box, and deoxygenated extra-dry solvents were used to avoid catalyst deactivation.

X-ray absorption fine-structure (XAFS) spectroscopy

XAFS beamlines: Soft X-ray absorption near-edge structure (XANES) spectra at the Cr $L_{2,3}$-edge (570–590 eV) were measured on beamline U49/2-PGM1 of BESSY (Berlin, Germany). Details of the soft X-ray measurements and equipment can be found in the literature.[25] Two collector plates served as detectors of the ionized gas and of the subsequent

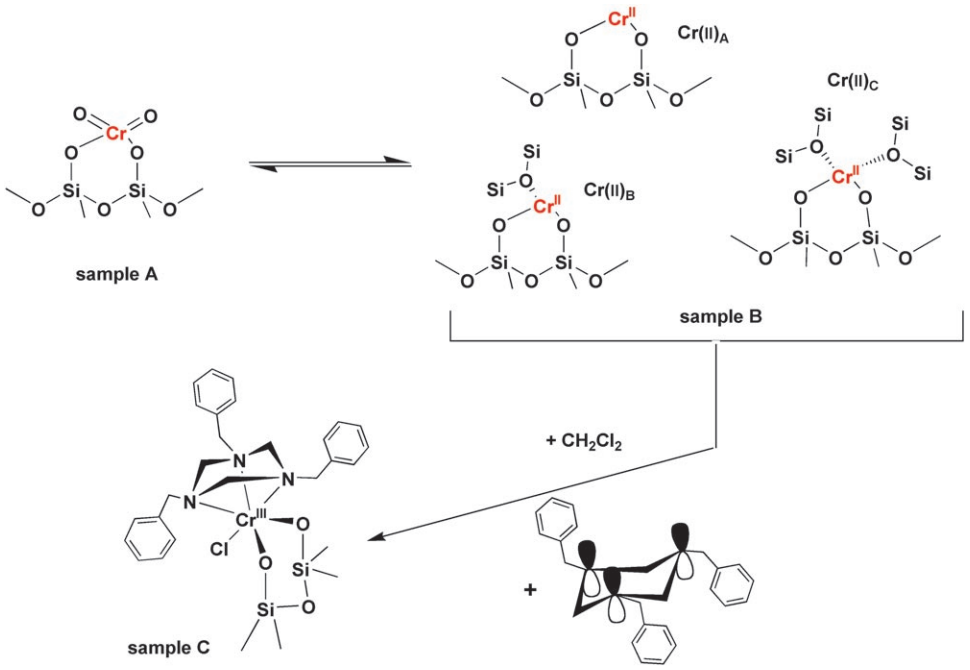

Scheme 1. Assembly of a single-site catalyst starting from a Phillips-type catalyst (simplified structures of Cr^{II} sites were used).

nonradiative decay of the core hole. The spectral resolution of the monochromator was 0.2 eV. Multiple scans were collected under 2.5 mbar He and averaged. XAFS measurements with hard synchrotron radiation were carried out at the Cr K-edge (5989 eV) on beamline E4 of HASYLAB (Hamburg, Germany) and on beamline BM26A of the ESRF (Grenoble, France). The positron storage ring at HASYLAB operated at 4.4 GeV with an average current of 120 mA. Beamline E4 was equipped with a Si(110) monochromator. Higher-order harmonics were eliminated by using a stabilization feedback control system. The fluorescence experimental setup consisted of a 7-pixel Si(Li) detector. The electron storage ring at ESRF operated at 6 GeV with a maximum current of 200 mA, and the higher-order harmonics were effectively rejected by using mirrors. A double-crystal Si(111) water-cooled monochromator was used. A 9-pixel Ge detector collected the fluorescence signal. In transmission mode, gas-ionization detectors were used. The energy steps for measurements in the XANES region were 0.3 eV at HASYLAB and 0.5 eV at ESRF.

XAFS data collection: The soft X-ray data were collected at RT and the 3.2 mbar He atmosphere was maintained during acquisition of the spectra. The hard X-ray data were measured at 77 K. Samples were pressed as self-supported discs and placed in a specially designed extended X-ray absorption fine-structure spectroscopy (EXAFS) cell,[26] then measured in either fluorescence mode (for Cr-diluted samples) or transmission mode (for reference compounds). For sample B, the in situ measurements of the Cr K-edge XANES spectra were carried out under a continuous flow of pure CO at 400 °C. The in situ experiments of sample C were recorded under He atmosphere with a time resolution of 20 min. The energy scale was calibrated by measuring the Cr K-edge of the metallic foil.

XAFS data analysis: All XANES spectra were normalized at 1 and the edge position was chosen, for consistency reasons, at 0.5 of the normalized intensity. To extract quantitative information from the Cr L-edge it was necessary to simulate the spectra. The MULTIPLET program[27,28] performs charge-transfer multiplet calculations combining atomic multiplet theory, crystal field theory, and many-body model Hamiltonians. This approach takes into account electronic Coulomb interactions, spin-orbit coupling on every shell and treats the geometry of the absorbing atom through a combination of a crystal field potential and a mixture of coupled configurations, for example, to model the metal-to-ligand charge transfer (MLCT). The XANES spectra of the Cr L-edge were calculated from the sum of all possible transitions for an electron moving from the 2p level to a 3d level.

EXAFS data analysis: EXAFS data analysis was carried out using the XDAPW2 code developed by Vaarkamp et al.[29] The pre-edge was subtracted by using a second-order polynomial. The edge position was calibrated by taking the second derivative of a Cr-foil spectrum and determining the position of the first inflection point. Normalization was carried out by dividing the data by the height of the absorption at 50 eV above the absorption edge. The background was subtracted by employing cubic spline routines with a continuously adjustable smooth parameter.[30] This yielded the normalized oscillatory part of the XAFS data, for which all the contributions to the spectrum, including the AXAFS, were maximized.[30] The EXAFS data-analysis program XDAPW2 allows one to perform multiple-shell fitting in R space by minimizing the residuals between both the absolute and the imaginary part of the Fourier transforms of the data and the fit. R-space fitting has important advantages over the usually applied fitting in k space and is extensively discussed in a paper by Koningsberger et al.[30] The variances of the magnitude and imaginary part of the Fourier transforms of fit and data were calculated according to Equation (1):

$$\text{variance} = \frac{\int [\mathrm{FT}(k^n\chi_{\text{model}}) - \mathrm{FT}(k^n\chi_{\text{exptl}})]^2 \mathrm{d}R}{\int [\mathrm{FT}(k^n\chi_{\text{exptl}})]^2 \mathrm{d}R} \times 100 \quad (1)$$

The difference-file technique was applied together with phase-corrected Fourier transforms to resolve the different contributions in the EXAFS data.[30] If the experimental spectrum is composed of different contributions, then:

$$\text{exptl data} = \sum_{i=1}^{N} (\text{fit})_i \quad (2)$$

in which $(\text{fit})_i$ represents the fitted contribution of the coordination shell i and N is the number of shells. For each individual contribution, Equation (3) should then logically be valid:

$$(\text{fit})_j = \text{exptl data} - \sum_{i=1 \text{ and } i\neq j}^{N} (\text{fit})_i \quad (3)$$

The right-hand side of Equation (3) is further denoted as the difference file of shell j. A good fit is obtained only if the total fit and each individual contributing coordination shell describe correctly the experimental EXAFS and the difference file, respectively. In this way, not only the total EXAFS fit, but also the individual fits of all separate contributions can be determined reliably. In this study, the statistical significance of a contribution was checked by comparing the amplitude of $(\text{fit})_j$ with the noise level present in the experimental data. The data discussed in this paper were analyzed by using a multiple-shell R-space fit with k^1 and k^3 weightings, $\Delta k = 3$–11 Å^{-1} and $\Delta R = 1.5$–3.5 Å. The validity of the fit was checked in all k weightings (k^n, for which $n = 0$, 1, 2, and 3). The applied fit ranges allowed the number of independent parameters (N_{ind}) to be 13.4, according to the Nyquist theorem:[31]

$$N_{\text{ind}} = \frac{2\Delta R \Delta k}{\pi} + 2 \quad (4)$$

Data for the Cr–O, Cr–N, Cr–C, and Cr–Cl phase shifts and backscattering amplitudes were obtained from calculations using the FEFF8 code.[32,33] Table 1 gives the input parameters of the FEFF8 code. The theoretical references were calibrated on experimental EXAFS data of Cr_2O_3, $CrCl_3$, and $CrCl_3$–TAC by using an R-space fit. The input parameters of the FEFF8 code were adjusted until the experimental reference was fitted with $\Delta\sigma^2 = 0$, $\Delta E_0 = 0$, with distance and coordination number taken to be the same as the crystallographic data of the reference compounds. Further details of the calibration procedure are given in the Supporting Information.

Table 1. FEFF8 input parameters used for the calculation of phase shifts and backscattering amplitudes.

Atom pair	Experimental reference	N	R [Å]	σ^2 [Å^2]	$S_0{}^2$	V_r [eV]	V_i [eV]
Cr–O	Cr_2O_3	3	1.900	0.0005	1.0	−13	1.0
Cr–N	$CrCl_3$–TAC	3	2.095	0.0020	1.0	−8	1.0
Cr–Cl	$CrCl_3$	6	2.330	0.0016	0.7	−3.5	1.0
Cr–C	$CrCl_3$–TAC	3	2.615	0.0080	1.0	1.1	1.0

DFT calculations: Quantum-chemical calculations were performed by using the GAMESS-UK program. Exchange-correlation energy was added to the calculations by using the B3LYP density functional.[34,35] All calculations were performed with the CERNBL basis set and accompanying ECPs from the EMSL basis-set database. The structures of the clusters were optimized to a maximum gradient of 4.4×10^{-4}. After optimization, a natural-orbital population analysis was conducted with the natural bond orbital (NBO) module in GAMESS-UK.[34,36]

Results

X-ray absorption near-edge structure (XANES) of Cr L- and K-edge: Figure 1 shows the Cr K-edge XANES spectra of the starting catalyst (sample A) and of the catalyst after reduction with CO (sample B). Basically, reference chro-

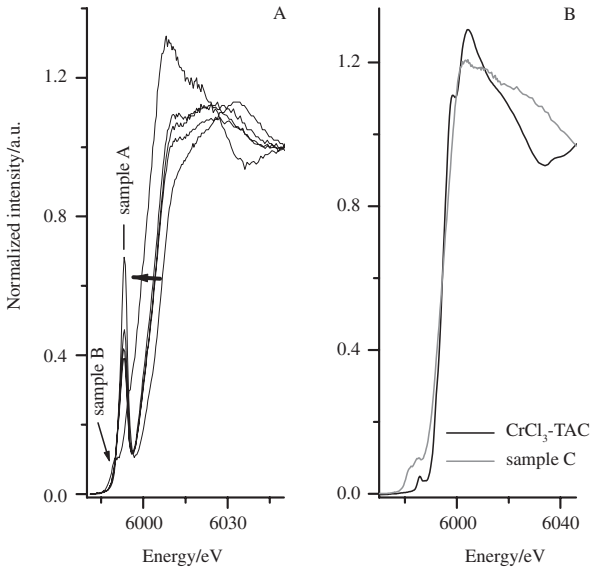

Figure 1. A) Cr K-edge XANES spectra of sample A, converted in situ into sample B through the reduction of surface chromates to surface-anchored Cr^{2+} species. The intense pre-edge peak of the tetrahedral sample A decreases gradually and a low-intensity peak appears for the octahedral sample B. The edge transition of sample A is shifted towards lower energies in sample B as indicated by the arrow. Spectra were collected after each 20 min. B) XANES spectra of sample C and its reference complex $CrCl_3$–TAC.

mate compounds present similar Cr K-edge XANES spectra and, therefore, we can conclude that sample A consists mainly of surface chromates, although the presence of traces of polychromates cannot be excluded. One reference for chromate species together with other reference compounds, as well as the most important XANES features of samples A, B, and C are listed in Table 2.

Under CO atmosphere and at 400 °C, sample A is reduced in situ to sample B. In Figure 1A, the Cr K-edge is plotted as a function of time during the progressive conversion of sample A to sample B. The spectrum of sample A exhibits a sharp and intense pre-edge peak at 5993.6 eV, known to be characteristic for the dipole-forbidden transition 1s→3d in chromium compounds with an oxidation state of six and tetrahedral geometry. Due to the reduction with CO, the intense pre-edge peak of sample A is gradually diminished until it is completely replaced by a very low-intensity peak positioned at 5990.1 eV. This new peak indicates a change in the symmetry of the Cr absorber towards octahedral. The edge transition is also shifted to lower energies, from 6006.5 eV (sample A) to 5999.4 eV (sample B), indicating an average oxidation state of between two and three.[37] Apart from the edge shift, the intense shoulder is indicative for the conversion of the oxidation state six in sample A towards oxidation state two in sample B.[38]

Figure 2 presents the Cr $L_{2,3}$-edge spectra of sample C and those of the reference compound, Cr_2O_3. The $L_{2,3}$-edge X-ray absorption spectra were analyzed by performing charge-transfer multiplet calculations, which yielded information on the ground-state electronic structure of the metal ion. Only a few studies exist in the literature on the $L_{2,3}$-edges of chromium systems,[39–44] and all involve bulk oxides. Systems with low concentrations of chromium, as is the case for sample C, have not yet been reported. The close similarity of the spectra of sample C and Cr_2O_3 indicates that both chromium systems are present in a similar electronic state. The Cr in Cr_2O_3 occupies a (distorted) octahedral position and the ligand field multiplet simulations yield a Cr^{III} ground state that has ~80% $3d^3$ character and ~20% $3d^4L$ character, in which a hole exists on the oxygen neighbors.[45,46] The (overall) ligand field splitting is 2.0 eV. The charge-transfer fit of the sample C is less accurate, due mainly to variations in the background and to the measurements being made in a gas-phase environment. Nevertheless, it is clear that the ground state of chromium is very similar to that of Cr_2O_3, in which the lower intensity of the first peak of the L_3-edge suggests a smaller crystal field, of the order of 1.5 eV. Thus, Cr is found in a valence state of three in sample C, which is in agreement with the XANES analysis at the Cr K-edge.

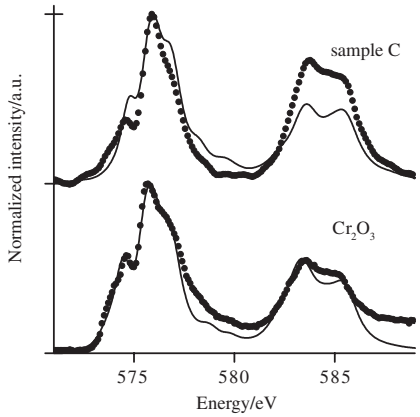

Figure 2. XANES spectra of the Cr $L_{2,3}$-edge of sample C (top, dotted region) and Cr_2O_3 (bottom, dotted region) together with the simulated spectra obtained with charge-transfer multiplet calculations.

Table 2. Cr K-edge XANES features of the catalytic material and reference compounds studied.

Compound	Coordination geometry	Oxidation state	Cr K-edge position [eV]	References
Cr foil[a]	cubic	0	5990.7	–
sample A[a]	tetrahedral	+6	6006.5	[37, 53–55]
sample B[a]	distorted octahedral	>+2	5999.0	[52]
sample C[a]	distorted octahedral	+3	5994.2	–
$CrCl_3$–TAC[a]	octahedral	+3	5994.5	–
CrN[a]	octahedral	+3	5994.0	–
CrO_3	octahedral	+6	6008.0	[53–55]
Cr_2O_3	octahedral	+3	5999.5	[51, 53–55]
$CaCrO_4$	tetrahedral	+6	6008.7	[51]

[a] Our own measurements compared with the literature data, where possible.

Extended X-ray absorption fine-structure (EXAFS) data analysis: The XANES spectra and the EXAFS spectra with the corresponding FTs (k^1, $\Delta k = 3$–13 Å^{-1}) of the newly assembled Cr/SiO_2 catalyst (sample C) and the $CrCl_3$–TAC reference compound are shown in Figure 1B and Figure 3,

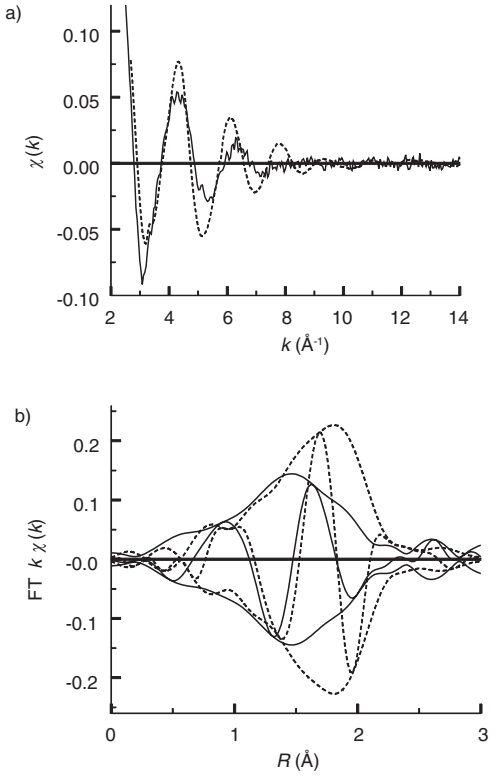

Figure 3. a) EXAFS spectra and b) Fourier transform (k^1, $\Delta k = 3$–13 Å^{-1}) of the Cr/SiO_2 sample C (solid line) and reference complex $CrCl_3$–TAC (dotted line)

respectively. The structural properties of the Cr/SiO_2 catalysts and the $CrCl_3$–TAC are not the same. From a synthetic point of view, it is very likely that the TAC ligand will be attached to Cr, but it is also logical to assume that Cr is linked to the support through a Cr−O bond. Moreover, during the preparation, a chlorinated solvent CH_2Cl_2 was used and the crucial question to be answered is whether Cl is coordinated to Cr in the final Cr complex. The resemblance of sample C XANES data with that of the reference $CrCl_3$–TAC (see Figure 1B) strongly suggests a distorted octahedral-like coordination. Therefore, the EXAFS data were analyzed by using Cr–O, Cr–Cl, and Cr–N ($N = 3$; $R = 2.095$ Å) and Cr–C ($N = 3$; $R = 2.615$ Å) coordinations, thereby assuming that 1) the TAC stays intact as ligand, 2) the complex is anchored by support oxygen bonds, and 3) Cl is coordinated to the final Cr complex.

The R-space fit (k^1, $\Delta k = 3$–13 Å^{-1}, $\Delta R = 0.5$–2.5 Å) was applied with four coordination shells, thereby fixing the coordination number and coordination distance of Cr–N and Cr–C in the Cr–TAC coordination. This leads to a total of 12 fit parameters. The fit is allowed, as the number of fit parameters is still lower than the number of allowed independent parameters (14.7), calculated according to the Nyquist theorem [Eq. (4)]. The final fit results of the four-shell fit are given in Table 3. The variances of the R-space fit are acceptable. The fits in R space obtained by using both k^1 and k^3 weightings are plotted in Figure 4 with a dotted line. This fit in both weightings adequately describes the data. In Figure 5 the Fourier transforms of the difference files of all four contributions (solid lines) are plotted with the corresponding Fourier transforms of the fitted contributions (dotted lines). The intensity of the different contributions is in the order Cr–O > Cr–N > Cr–Cl > Cr–C. The fitted Cr–O and Cr–N contributions are described closely by the corresponding difference files.

Table 3. Fit result for the experimental data obtained by using the theoretical references. The fit was performed in R space, FT[a] (k^1, $\Delta R = 0.5$–2.5 Å, $\Delta k = 3$–13 Å^{-1}). Number of free parameters is 14.7.

Shell	Absorber–backscatterer	N	R [Å]	$\Delta\sigma^2$ [Å^2]	ΔE_0 [eV]	Calculated distances [Å]
1	Cr–O	2.0	1.91	0.003	−8.4	1.88
2	Cr–N	3.0[b]	2.10[b]	0.007	4.0	2.20
3	Cr–Cl	1.0	2.28	0.012	−12.8	2.34
4	Cr–C	3.0[b]	2.62[b]	0.018	10.6	2.69

[a] Variances: ImFT = 0.4; AbsFT = 0.2. [b] Fixed input parameter.

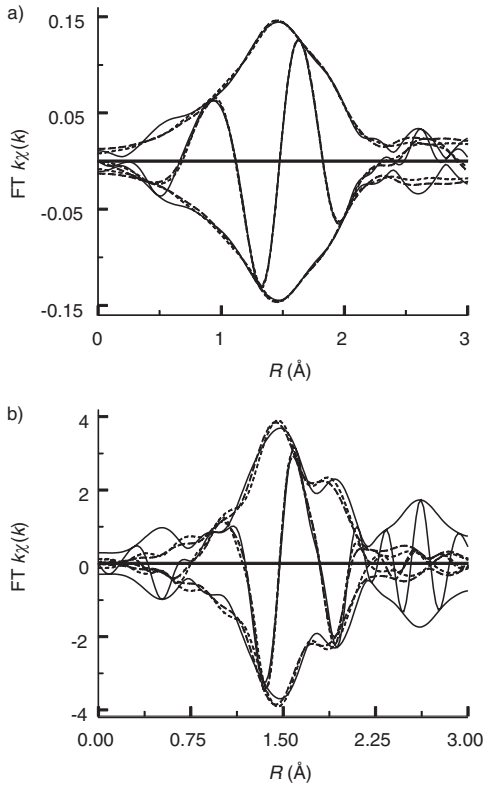

Figure 4. a) k^1-weighted and b) k^3-weighted Fourier transform ($\Delta k = 3$–13 Å^{-1}) of raw EXAFS data of the Cr/SiO_2 sample C (solid line) and total fit with four shells (dotted lines).

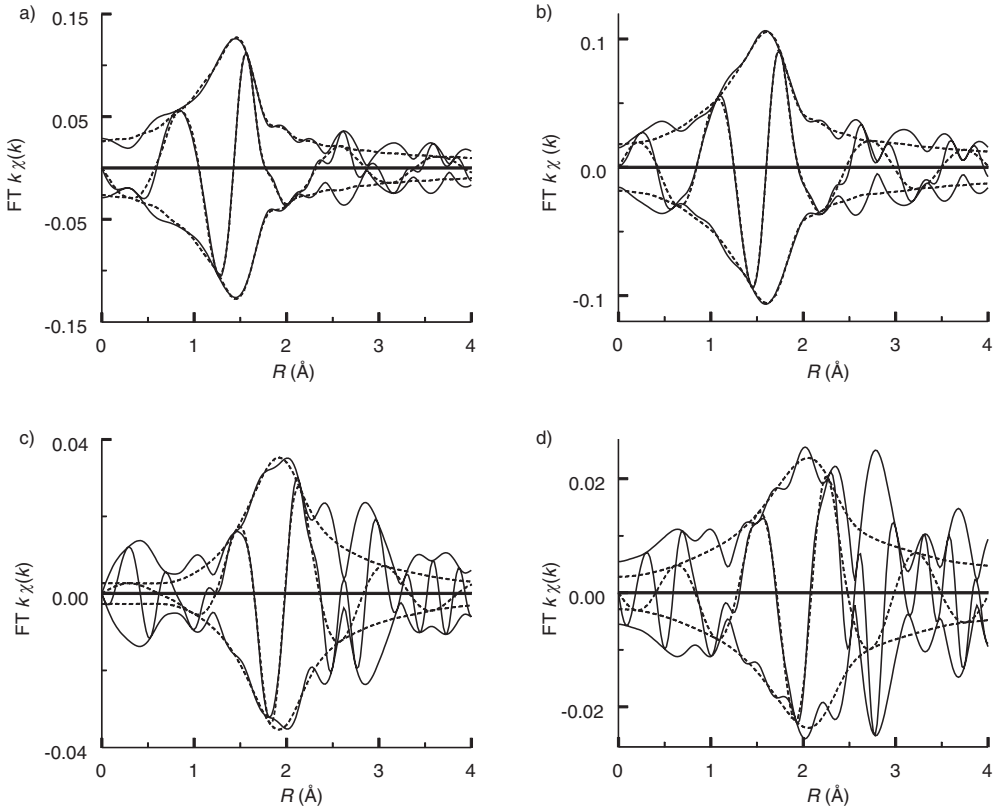

Figure 5. Fourier transforms (k^1, $\Delta k = 3$–13 Å^{-1}) of difference files (solid lines) and fits (dotted lines) of a) Cr–O, b) Cr–N, c) Cr—Cl, and d) Cr–C.

Ab initio calculations: The natural bond orbital (NBO) analysis[36,47] of the optimized structure results in three unpaired electrons in d-orbitals of the Cr atom and shows a total charge on Cr of 1.2 after coordination of all ligands. The DFT optimization calculation of sample C resulted in internal distances that compare very well with the results from the EXAFS fit, as can be seen in Table 3. Although the calculated Cr–N distances are slightly greater than the radial distances proposed by EXAFS, this is due to the weak coordination of the TAC ligand. In fact, DFT cannot describe this effect accurately. The remaining distances match well with the EXAFS data.

Discussion

We started our systematic structural investigation from the classical Phillips-type system (sample A). This material was reduced by CO to yield polymerization-active species, mainly Cr^{II} sites (sample B), on which the new active sites were assembled (sample C). The conversion of sample A into sample B involves a typical reduction of surface chromates towards highly unsaturated Cr^{II} sites, which is already well known.[2,3,8–12,48,49] Nevertheless, some chromium reference compounds in different oxidation states were also recorded and analyzed.[50] On the other hand, the conversion of sample B into sample C is completely unknown and requires further extensive investigation. The reference compounds were selected to have local environments with at least some similarity to the surface species of samples A, B, and C.

The results obtained for samples A and B are in good agreement with the Cr K-edge literature data,[37,51–55] although some studies are contradictory,[56,57] depending on the analysis method used by the respective group.

Based on the results shown in Table 2, we can conclude that the average oxidation state of sample C should be close to three, because the edge position of sample C is close to that of other chromium compounds in oxidation state three. The most appropriate comparison that can be made for sample C regarding its oxidation state and its local geometry is nevertheless with the $CrCl_3$–TAC reference compound. The Cr K-edge XANES spectra of these compounds are compared in Figure 1B. The good overlap of the edge position in these compounds confirms an equal oxidation state, that is, +3. It is also evident that the octahedral geometry is dominant in both systems. However, the asymmetrical shape of the pre-edge peak of sample C indicates a distorted geometry in contrast to the regular octahedral geometry found for the $CrCl_3$–TAC complex.

The proposed structure for the newly prepared Cr/SiO_2 catalyst (sample C) based upon the final EXAFS fit and ab initio calculation is shown in Scheme 1. The coordination of sample C is a distorted octahedron, as already predicted by XANES data. The analyzed Cr–N and the Cr–C distances demonstrate that during the preparation procedure, the TAC ligand does indeed coordinate to the supported Cr species. The Cr complex is anchored to the support by two Cr–

$O_{support}$ bonds with a coordination distance of 1.91 Å, almost identical to the first shell distance, as found in Cr_2O_3. One Cl neighbor at a distance of 2.28 Å was needed to make the fit acceptable. The difference files presented in Figure 5 made clear that strong antiphase effects are present between the different contributions. The imaginary parts of the FTs of the Cr–N and Cr–Cl/Cr–C also demonstrate the antiphase behavior of these contributions. A fit procedure using both weightings is necessary to unravel these interference effects, because antiphase behavior affects k^1 and k^3 weightings differently. A close inspection of the difference file and the fit of the Cr–Cl and Cr–C contribution (see Figure 5) shows that nonfitted higher-shell peaks are present, which interfere strongly with the fitted EXAFS on the high R side of the FT peak.

In conclusion, the EXAFS analysis indicates the presence of two oxygen scatterers as the closest atoms to the chromium absorber. The obtained distance of 1.9 Å is in full agreement with the Cr–O distance obtained for the first coordination shell, for example, Cr^{III} (O_h) in Cr_2O_3. In addition, three nitrogen scatterers and three carbon scatterers found at 2.08 and 2.64 Å, respectively, indicate that the TAC ligand is indeed attached to chromium through three nitrogen atoms. Finally, one chlorine scatterer at a distance of 2.28 Å was found, which completes the octahedral geometry of the chromium center. In Table 3, the average distances between the chromium absorber and the closest detected scatterers are shown.

Ab initio DFT calculations validate the local structure of sample C, as proposed by the EXAFS analysis. In this respect, the calculated distances listed in Table 3 are conclusive. The value for the unpaired electrons of Cr and the resulting oxidation state are in good agreement with the Cr^{III} oxidation state found by XANES analyses.

Conclusion

The detailed XAFS structural analysis has revealed that:

1) The average oxidation state of sample A has changed subsequently from six to two in sample B and, during the assembling procedure, from two to three in sample C.
2) The octahedral coordination geometry of chromium in sample C is preserved after the assembling process, but this becomes highly distorted, as indicated by scatterers at different distances.
3) Cr is linked to the TAC ligand, to the silica lattice and to a chloride ligand, indicating the formation of a new site.

The molecular structure of sample C obtained after XAFS analysis by using an R-space fit up to $R = 2.5$ Å, together with the proposed assembling process, is shown in Scheme 1. Consequently, strong coordinating ligands are able to mediate subtly the spatial and electronic structure of the heterogeneous sites, in our case, supported Cr^{II}.

This study shows that sample B can bind electron-donor ligands, that is, rigid TAC rings, as well as electron-accepting ligands (i.e., chloride) to reach a more-stable electronic configuration of chromium. Electron-accepting and -donating processes should appear internally as a prime condition for the assembly of sample C. Indeed, after the assembly process, a single-site heterogeneous Cr-based site is obtained. In this respect, we assume that the coordination of chloride and TAC ligands to Cr^{II} sites had modified significantly the electronic and spatial environment of chromium sites, leading to uniform structures. Most likely, the displacement of the weakly coordinated siloxane ligands by the more-strongly coordinated ones, the TAC ligand and chloride ligands, respectively, forces the sunken Cr^{II} sites of sample B to ascend to the surface. Thereby, the structural heterogeneity of the resultant system is reduced considerably by erection of new molecular structures on the surface, so that it becomes basically a monodisperse system. To the best of our knowledge, this approach regarding the reduction in complexity of a heterogeneous catalytic system is reported here for the first time, but it should, in principle, also apply for other metal-oxide systems.

Acknowledgements

This work was supported by grants from ATOFINA Research and NWO CW-VICI. The authors thank the synchrotrons staff for their help, as well as Axel Knop-Gericke and Michael Hävecker from the Fritz-Haber Institute for their support during the Cr $L_{2,3}$-edge measurements. We also acknowledge the use of the supercomputer time on TERAS, SARA (The Netherlands). The LanL2 basis set was obtained from the EMSL Gaussian Basis Set database.

[1] B. M. Weckhuysen, I. E. Wachs, R. A. Shoonheydt, *Chem. Rev.* **1996**, *96*, 3327–3349, and references therein.
[2] B. M. Weckhuysen, R. A. Schoonheydt, *Catal. Today* **1999**, *51*, 215–221.
[3] B. M. Weckhuysen, R. A. Schoonheydt, *Catal. Today* **1999**, *49*, 441–451.
[4] A. Zecchina, E. Garrone, G. Ghiotti, C. Morterra, E. Borello, *J. Phys. Chem.* **1975**, *79*, 966–972.
[5] A. Zecchina, G. Spoto, G. Ghiotti, E. Garrone, *J. Mol. Catal.* **1994**, *86*, 423–446.
[6] A. Zecchina, D. Scarano, S. Bordiga, G. Spoto, C. Lamberti, *Adv. Catal.* **2001**, *46*, 265–397.
[7] A. Zecchina, G. Spoto, S. Bordiga, *Phys. Chem. Chem. Phys.* **2005**, *7*, 1627–1642.
[8] E. Groppo, C. Lamberti, S. Bordiga, G. Spoto, A. Zecchina, *Chem. Rev.* **2005**, *105*, 115–183, and references therein.
[9] M. P. McDaniel, *J. Catal.* **1982**, *76*, 29–36.
[10] M. P. McDaniel, *J. Catal.* **1982**, *76*, 37–47.
[11] M. P. McDaniel, *J. Catal.* **1982**, *76*, 17–28.
[12] M. P. McDaniel, *Adv. Catal.* **1985**, *33*, 47–98.
[13] K. Ziegler, E. Holzkamp, H. Martin, H. Breil, *Angew. Chem.* **1955**, *67*, 541–547.
[14] E. Groppo, C. Lamberti, G. Spoto, S. Bordiga, G. Magnacca, A. Zecchina, *J. Catal.* **2005**, *236*, 233–244.
[15] P. C. Thune, C. P. J. Verhagen, M. J. G. vandenBoer, J. W. Niemantsverdriet, *J. Phys. Chem. B* **1997**, *101*, 8559–8563.
[16] P. C. Thune, J. Loos, P. J. Lemstra, J. W. Niemantsverdriet, *J. Catal.* **1999**, *183*, 1–5.

[17] P. C. Thune, J. Loos, A. M. de Jong, P. J. Lemstra, J. W. Niemantsverdriet, *Top. Catal.* **2000**, *13*, 67–74.
[18] P. C. Thune, J. W. Niemantsverdriet, Israel J. Chem. **1998**, *38*, 385–391.
[19] P. C. Thune, R. Linke, W. J. H. van Gennip, A. M. de Jong, J. W. Niemantsverdriet, *J. Phys. Chem. B* **2001**, *105*, 3073–3078.
[20] P. C. Thune, J. Loos, D. Wouters, P. J. Lemstra, J. W. Niemantsverdriet, *Macromol. Symp.* **2001**, *173*, 37–52.
[21] P. G. Di Croce, F. Aubriet, P. Bertrand, P. Rouxhet, P. Grange, *Stud. Surf. Sci. Catal.* **2002**, *143*, 823–835.
[22] P. G. Di Croce, F. Aubriet, R. Chety-Gimondo, J. F. Muller, P. Grange, *Rapid Commun. Mass Spectrom.* **2004**, *18*, 601–608.
[23] P. Bodart, C. Nenu, B. M Weckhuysen, WO 2005/082815 A1 application.
[24] C. N. Nenu, B. M. Weckhuysen, *Chem. Commun.* **2005**, 1865–1867.
[25] A. Knop-Gericke, M. Havecker, T. Schedel-Niedrig, R. Schlogl, *Top. Catal.* **2000**, *10*, 187–198.
[26] F. W. H. Kampers, T. M. J. Maas, J. Grondelle, P. Brinkgreve, D. C. Koningsberger, *Rev. Sci. Instrum.* **1989**, *60*, 2635–2638.
[27] F. M. F. de Groot, *J. Electron Spectrosc. Relat. Phenom.* **1994**, *67*, 529–622.
[28] F. M. F. de Groot, *Coord. Chem. Rev.* **2005**, *249*, 31–63.
[29] M. Vaarkamp, J. C. Linders, D. C. Koningsberger, *Physica B* **1995**, *208*/209, 159–160.
[30] D. C. Koningsberger, B. L. Mojet, G. E. van Dorssen, D. E. Ramaker, *Top. Catal.* **2000**, *10*, 143–155.
[31] E. A. Stern, *Phys. Rev. B* **1993**, *48*, 9825–9827.
[32] A. L. Ankudinov, B. Ravel, J. J. Rehr, S. D. Conradson, *Phys. Rev. B* **1998**, *58*, 7565–7576.
[33] J. Mustre de Leon, J. J. Rehr, S. I. Zabinski, R. C. Albers, *Phys. Rev. B* **1991**, *44*, 4146–4156.
[34] M. F. Guest, I. J. Bush, H. J. J. van Dam, P. Sherwood, J. M. H. Thomas, J. H. van Lenthe, R. W. A. Havenith, J. Kendrick, *Mol. Phys.* **2005**, *103*, 719–747.
[35] R. H. Hertwig, W. Koch, *Chem. Phys. Lett.* **1997**, *268*, 345–351.
[36] F. Weinhold, J. E. Carpenter, *The Structure of Small Molecules and Ions*, Plenum, New York, **1988**, pp. 227–236.
[37] E. Groppo, C. Prestipino, F. Cesano, F. Bonino, S. Bordiga, C. Lamberti, P. C. Thüne, J. W. Niemantsverdriet, A. Zecchina, *J. Catal.* **2005**, *230*, 98–108.
[38] S. R. Sutton, K. W. Jones, B. Gordon, M. L. Rivers, S. Bajt, J. V. Smith, *Geochim. Cosmochim. Acta* **1993**, *57*, 461–468.
[39] C. Theil, J. van Elp, F. Folkmann, *Phys. Rev. B* **1999**, *59*, 7931–7936.
[40] M. F. Lopez, A. Gutierrez, M. C. Garcia-Alonso, M. L. Escudero, *J. Mater. Res.* **1998**, *13*, 3411–3416.
[41] M. F. Lopez, A. Gutierrez, C. L. Torres, J. M. Bastidas, *J. Mater. Res.* **1999**, *14*, 763–770.
[42] M. F. Lopez, A. Gutierrez, F. J. Perez, M. P. Hierro, F. Pedraza, *Corros. Sci.* **2003**, *45*, 2043–2053.
[43] J. M. Bastidas, M. F. Lopez, A. Gutierrez, C. L. Torres, *Corros. Sci.* **1998**, *40*, 431–438.
[44] O. C. Rogojanu in *Stabilizing CrO by Epitaxial Growth*, PhD thesis, University of Groningen, Groningen, **2003**, p. 125.
[45] F. M. F. de Groot, *J. Electron Spectrosc. Relat. Phenom.* **1998**, *92*, 207–211.
[46] F. M. F. de Groot, *Top. Catal.* **2000**, *10*, 179–186.
[47] A. E. Reed, L. A. Curtiss, F. Weinhold, *Chem. Rev.* **1988**, *88* 899–926.
[48] B. M. Weckhuysen, R. A. Schoonheydt, J. M. Jehng, I. E. Wachs, S. J. Cho, R. Ryoo, S. Kijlstra, E. Poels, *J. Chem. Soc. Faraday Trans.* **1995**, *91*, 3245–3253.
[49] M. P. McDaniel in *Handbook of Heterogeneous Catalysis, Vol. 5* (Eds.: G. Ertl, H. Knözinger, J. Weitkamp), VHC, Weinheim, **1997**, p. 2400.
[50] M. Fernandez-Garcia, *Catal. Rev.* **2002**, *44*, 59–121.
[51] I. Arcon, B. Mirtic, A. Kodre, *J. Am. Ceram. Soc.* **1998**, *81*, 222–224.
[52] A. J. Berry, H. S. C. O'Neill, *Am. Mineral.* **2004**, *89*, 790–798.
[53] A. Ellison, G. Diakun, P. Worthington, *J. Mol. Catal.* **1988**, *46*, 131–149.
[54] A. Ellison, T. L. Overton, L. Bencze, *J. Chem. Soc. Faraday Trans.* **1993**, *89*, 843–849.
[55] A. Ellison, T. L. Overton, *J. Mol. Catal.* **1994**, *90*, 81–86.
[56] A. Pantelouris, H. Modrovw, M. Pantelouris, J. Hormes, D. Reinen, *Chem. Phys.* **2004**, *300*, 13–22.
[57] D. Wei, N. Yao, G. L. Haller, *Catal. Rev. Sci. Eng.* **1998**, 239–244.

Received: January 19, 2006
Published online: April 6, 2006

